

## $\alpha$ clustering with a hollow structure: Geometrical structure of $\alpha$ clusters from platonic solids to fullerene shape

Akihiro Tohsaki<sup>1</sup> and Naoyuki Itagaki<sup>2</sup>

<sup>1</sup>*Research Center for Nuclear Physics (RCNP), Osaka University, 10-1 Mihogaoka, Ibaraki, Osaka 567-0047, Japan*

<sup>2</sup>*Yukawa Institute for Theoretical Physics, Kyoto University, Kitashirakawa Oiwake-Cho, Kyoto 606-8502, Japan*



(Received 29 August 2017; revised manuscript received 13 October 2017; published 10 January 2018)

We study  $\alpha$ -cluster structure based on the geometric configurations with a microscopic framework, which takes full account of the Pauli principle, and which also employs an effective internucleon force including finite-range three-body terms suitable for microscopic  $\alpha$ -cluster models. Here, special attention is focused upon the  $\alpha$  clustering with a hollow structure; all the  $\alpha$  clusters are put on the surface of a sphere. All the platonic solids (five regular polyhedra) and the fullerene-shaped polyhedron coming from icosahedral structure are considered. Furthermore, two configurations with dual polyhedra, hexahedron-octahedron and dodecahedron-icosahedron, are also scrutinized. When approaching each other from large distances with these symmetries,  $\alpha$  clusters create certain local energy pockets. As a consequence, we insist on the possible existence of  $\alpha$  clustering with a geometric shape and hollow structure, which is favored from Coulomb energy point of view. Especially, two configurations, that is, dual polyhedra of dodecahedron-icosahedron and fullerene, have a prominent hollow structure compared with the other six configurations.

DOI: [10.1103/PhysRevC.97.011301](https://doi.org/10.1103/PhysRevC.97.011301)

Carbon atoms play an essential role in composing molecular structure related to geometric configuration in organic chemistry. It is plausible that  $\alpha$  particles are in the same situation in nuclear structure as carbon atoms in molecular structure because of their strong binding energy and the dual role of the Pauli principle [1,2]. When two  $\alpha$  particles are at a distance from each other, the Pauli principle works attractively; on the other hand, the strong repulsion acts on approaching two  $\alpha$  particles. Not only cannot the  $\alpha$  cluster easily break down but also two  $\alpha$  particles have a resonance state around the threshold energy. We can point out that three  $\alpha$  clusters are loosely bound in making Borromean nucleus, which was predicted to be  $\alpha$ -cluster condensation [3,4].

Up to now, there have been many studies on the geometrical structure of  $\alpha$  clusters based on the microscopic frameworks, which employ effective internucleon forces and completely consider the Pauli principle simultaneously [5]. In particular, the Brink-Bloch model is one of the suitable tools for studying the geometric structure of  $\alpha$  clustering [6]. However, almost all the attempts have been restricted up to  $4N$  nuclei of  $(0p)$ -shell region. Furthermore, the employed effective internucleon force is different for every  $\alpha$ -type  $4N$  nuclei because we do not have appropriate ones to reproduce the physical quantities in the wide mass number region from  $\alpha$  particle to nuclear matter. For instance, the Volkov force [7], which is the most popular internucleon force, includes the Majorana strength as an adjustable parameter for every nucleus. Nevertheless, the saturation property for the nuclear matter cannot be reproduced.

Fortunately, the introduction of the finite-range three-body internucleon force can elegantly overcome the defects of internucleon force only with the two-body terms. The overall saturation property in the wide mass number region of  $4N$

nuclei is well explained by using an effective internucleon force with finite-range three-body terms related to the density dependency. The concepts of deciding the parameters in the effective internucleon force are as follows: (1) reasonable reproduction of the saturation property of  $\alpha$ ,  $^{16}\text{O}$ ,  $^{40}\text{Ca}$ , and nuclear matter, and (2) the reproduction of the phase shift of elastic  $\alpha$ - $\alpha$  scattering. In this report, we use Tohsaki F1 force [8] (we call F1). Recent report by one of the authors verifies the validity of the F1 force for the unified understanding of the  $^{12}\text{C}$  and  $^{16}\text{O}$  [9]. As a comparison, we show the results for the Brink-Boeker force [10] (referred as BB force), which has also no adjustable parameter but which cannot reproduce the saturation property except for  $\alpha$  particle and nuclear matter. Therefore, we think that F1 force is more reliable than BB force, but here we compare the results of two forces.

In this Rapid Communication, we show that  $\alpha$  clusters with geometric configurations create certain local energy pockets when they approach each other from large distances. This is because Coulomb repulsion is the most important factor at large distances, and formation of geometric configurations allows us to reduce this effect. The contribution of the nuclear interaction creates distinct local energy minimum points; on the other hand, the Pauli principle works repulsively after the touching inside the nuclear surface.

The importance of  $\alpha$  cluster structure has been pointed out also in the heavy mass region. For instance,  $\alpha$ -like four-body correlation is found to be important in explaining the  $\alpha$  decay [11]. The formation of  $\alpha$  cluster around the nuclear surface has been discussed in quite heavy Polonium isotopes for a long time [12]. Not only  $\alpha$  decays but also various types of cluster decays have been discussed in heavy nuclei [13]. Also, appearances of various geometric cluster configurations have been theoretically pointed out [14]. Furthermore, cluster

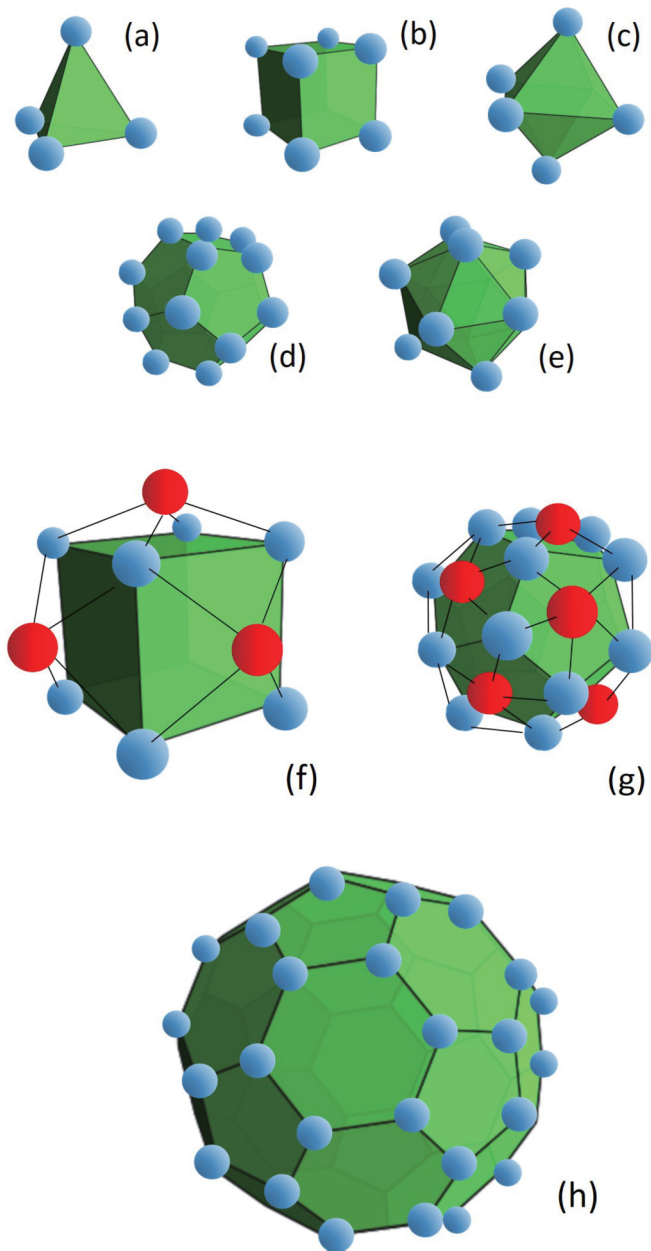


FIG. 1. Schematic figures for the prepared configurations, where vertices on the polyhedra show the positions of the  $\alpha$  clusters: (a) tetrahedron, (b) hexahedron (cube), (c) octahedron, (d) dodecahedron, (e) icosahedron, (f) hexahedron-octahedron, (g) dodecahedron-icosahedron, and (h) fullerene-shape polyhedron configurations.

structure has been studied from *ab initio* point of view [15]. In this study, we examine much multicenter  $\alpha$  cluster structure in even heavier regions.

As for the geometric configurations, first of all, we consider five Platonic solids (five regular polyhedra), of which vertices are positions of  $\alpha$  clusters. As schematically shown in Fig. 1, we prepare (a) tetrahedron, (b) hexahedron (cube), (c) octahedron, (d) dodecahedron, and (e) icosahedron configurations. They consist of 4, 8, 6, 20, and 12  $\alpha$  clusters corresponding to  $^{16}\text{O}$ ,  $^{32}\text{S}$ ,  $^{24}\text{Mg}$ ,  $^{80}\text{Zr}$ , and  $^{48}\text{Cr}$ , respectively. In addition, we

introduce their dual polyhedra, (f) hexahedron-octahedron and (g) dodecahedron-icosahedron; the latter is related to the rhombic triacontahedron, which is the basic seed of quasicrystal. Here, hexahedron-octahedron is a combination of two platonic solids, hexahedron and octahedron. In Fig. 1(f), blue balls are  $\alpha$  clusters at the vertices of hexahedron and red balls are  $\alpha$  clusters, which form pyramid shape together with the four nearest (blue)  $\alpha$  clusters. There are six red balls corresponding to the number of faces of hexahedron, and these six points form an octahedron shape. In total, we have 14  $\alpha$  clusters corresponding to  $^{56}\text{Ni}$ , and the distances from the origin are taken to be common for all the fourteen  $\alpha$ 's. Therefore, hexahedron and octahedron are inscribed in a common sphere. If we start with an octahedron shape and add  $\alpha$  clusters at the centers of the faces, formation of completely the same solid is achieved, and hexahedron and octahedron are considered as a pair (dual polyhedra). Another one is dodecahedron-icosahedron, which is the combination of dodecahedron and icosahedron. In Fig. 1(g), 20 blue balls are  $\alpha$  clusters at the vertices of dodecahedron, and 12 red  $\alpha$  clusters are added at the center of 12 faces, which form an icosahedron shape. We have 32  $\alpha$  clusters corresponding to  $^{128}\text{Gd}$ , and the distances from the origin are taken to be common for all the  $\alpha$ 's; dodecahedron and icosahedron are inscribed in a common sphere. If we start with an icosahedron shape and add  $\alpha$  clusters at the centers of the faces, the same solid is formed, and dodecahedron and icosahedron are considered as a pair (dual polyhedra). Note that tetrahedron is a self-dual polyhedron. If we apply the same procedure for the tetrahedron (adding  $\alpha$  clusters at the center of each surface and adjusting the distances from the origin to be the same as those of  $\alpha$ 's at vertices), it becomes hexahedron (cube), which is already included in the model as (b). Furthermore, we introduce (h) fullerene-shape polyhedron, which has 60  $\alpha$  clusters corresponding to  $^{240}\text{120}$ . The fullerene-shaped nucleus, whose atomic number is 120, belongs to the ultra-super-heavy region of nucleus. If the radius is very large, the configuration contains a big void inside of the sphere. In other words, we can imagine balloon-shaped nuclei and takes the rhombic triacontahedron and the fullerene configurations as their plausible candidates. In order to study the stability of the structure in this report, we show an adiabatic-energy curve with respect to the radius of the sphere, which is the only variational parameter to see the property of the breathing mode. Carrying out the angular momentum projection is unnecessary because of the symmetric shape of the sphere.

We employ Brink-Bloch-type wave function, which takes complete account of the Pauli principle:

$$\Psi(\rho) = \mathcal{A}\{\phi_1(\rho \mathbf{R}_1)\phi_2(\rho \mathbf{R}_2) \dots \phi_N(\rho \mathbf{R}_N)\}, \quad (1)$$

where  $\mathcal{A}$  is the antisymmetrization operator among all the nucleons. The  $N\alpha$  clusters are on the surface of the sphere with the radius  $\rho$  (fm), and the vectors  $\mathbf{R}_1, \dots, \mathbf{R}_N$  are the parameters on the dimensionless unit sphere. The  $k$ th  $\alpha$  cluster ( $k = 1, 2, \dots, N$ ) wave function is written by

$$\phi(\rho \mathbf{R}_k) = \prod_{i,j=1,2} \left( \frac{1}{\pi b^2} \right)^{\frac{3}{4}} \exp \left[ -\frac{1}{2b^2} (\mathbf{r}_k^{ij} - \rho \mathbf{R}_k)^2 \right] \chi_k^{ij}, \quad (2)$$

where  $b$  is the nucleon size parameter and  $\chi_k^{ij}$  is a spin isospin wave function. The vector  $\mathbf{r}_k^{ij}$  is the real physical coordinate for the nucleon, and  $i$  and  $j$  are labels for the spin and isospin, respectively, for the four nucleons in the  $k$ th  $\alpha$  clusters. The four nucleons in the  $k$ th  $\alpha$  cluster share the common Gaussian center,  $\rho \mathbf{R}_k$ . We prepare eight sets of  $\{\mathbf{R}_1, \dots, \mathbf{R}_N\}$  corresponding to the configurations in Fig. 1.

The norm and energy kernel matrix elements after carrying out the integration with respect to the real physical coordinates  $\{\mathbf{r}_k^{ij}\}$  are functions of variational parameter  $\rho$ :  $\langle \Psi(\rho') | \Psi(\rho) \rangle$  and  $\langle \Psi(\rho') | \hat{H} | \Psi(\rho) \rangle$ , where the Hamiltonian is given by

$$\hat{H} = -\frac{\hbar^2}{2M} \sum_i \nabla_i^2 - T_{\text{cm}} + \frac{1}{2!} \sum_{i,j} v_{ij}^{(c)} + \frac{1}{2!} \sum_{i,j} v_{ij}^{(2)} + \frac{1}{3!} \sum_{i,j,k} v_{ijk}^{(3)}. \quad (3)$$

The first and the second terms are the kinetic operator and the center of mass (c.m.) energy. The third is the Coulomb operator running over the protons, and the fourth and the fifth terms are the effective internucleon force separated by the two-body and three-body ones. The explicit form is written by the summation of Gaussian function:

$$v_{ij}^{(2)} = \sum_{l=1}^3 V_l^{(2)} \left\{ (1 - m_l^{(2)}) - m_l^{(2)} P_{ij}^\sigma P_{ij}^\tau \right\} \times \exp[-(\mathbf{r}_i - \mathbf{r}_j)^2 / \beta_l^2] \quad (4)$$

and

$$v_{ijk}^{(3)} = \sum_{l=1}^3 V_l^{(3)} \left\{ (1 - m_l^{(3)}) - m_l^{(3)} P_{ij}^\sigma P_{ij}^\tau \right\} \times \left\{ (1 - m_l^{(3)}) - m_l^{(3)} P_{jk}^\sigma P_{jk}^\tau \right\} \times \exp[-(\mathbf{r}_i - \mathbf{r}_j)^2 / \beta_l^2 - (\mathbf{r}_j - \mathbf{r}_k)^2 / \beta_l^2], \quad (5)$$

where the exchange operators for the spin and isospin parts are expressed by  $P_{ij}^\sigma$  and  $P_{ij}^\tau$ . The force strengths for two- and three-body are written by  $V_l^{(2)}$  and  $V_l^{(3)}$ , where their range parameters are given by  $\beta_l$ , and the Majorana strengths are  $m_l^{(2)}$  and  $m_l^{(3)}$ , where not only two-body but also three-body are given by the finite three-range description unlike the  $\delta$ -type zero-range force. The parameters for the range of the internucleon force are taken to be the same in two-body and three-body parts. On the other hand, the BB force does not have the three-body terms.

When all the position parameters  $\{\mathbf{R}_k\}$  are given, basically, the matrix elements of norm and Hamiltonian are analytically given. However, the summation over all the  $\alpha$  clusters still remains and this part is numerically performed in most of the conventional Brink-model calculations. Here we innovated a method to perform this summation analytically, which allows us to apply Brink model to much heavier nuclei. Here we estimate the adiabatic energy

$$E(\rho) = \frac{\langle \Psi(\rho) | \hat{H} | \Psi(\rho) \rangle}{\langle \Psi(\rho) | \Psi(\rho) \rangle} \quad (6)$$

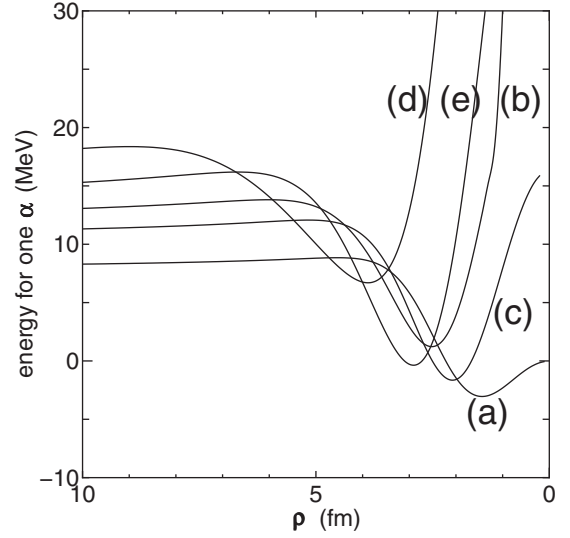


FIG. 2. Energy for one  $\alpha$  as a function of the radius ( $\rho$  in the text): (a) tetrahedron, (b) hexahedron (cube), (c) octahedron, (d) dodecahedron, and (e) icosahedron.

to find out the bulk property of the geometric configuration of  $\alpha$  clustering with a hollow structure. The diagonal part of the norm kernel has the following property depending on the antisymmetrization effect:

$$\lim_{\rho \rightarrow 0} \langle \Psi(\rho) | \Psi(\rho) \rangle = 0 \quad (7)$$

and we define the normalization as

$$\lim_{\rho \rightarrow \infty} \langle \Psi(\rho) | \Psi(\rho) \rangle = 1. \quad (8)$$

Therefore, it is reasonable to define the Pauli index as

$$p_i(\rho) = 1 - \langle \Psi(\rho) | \Psi(\rho) \rangle \quad (9)$$

for each configuration.

In Figs. 2 [for (a)–(e) in Fig. 1] and 3 [for (f)–(h) in Fig. 1], we show the adiabatic energy curves per  $\alpha$  for the case of F1 force. The horizontal axis is the radius  $\rho$  in Eq. (1), which starts with larger values and then decreases. The size parameter of single-nucleon wave function  $b$  is chosen to be 1.415 fm, leading to the minimum of the binding energy of  $\alpha$  particle, 27.500 MeV, reasonable comparison with the experimental value of 28.294 MeV; however, here the reference of the energy is taken as the  $N\alpha$  breakup energy. In all cases, the adiabatic energy curves have the energy barrier at larger distances and pocket at shorter distances.

In Table I, the physical quantities at the (A) energy barrier and (B) pocket positions in the case of F1 force are listed. Here, the acronym s.d. means the shortest distance of two  $\alpha$  clusters at the fixed radius of  $\rho$ , and P04(4), P08(6), P06(8), P20(12), P08-06(14), P12-20(32), and Ful(60) are configurations (a)–(h) in Fig. 1, where the values in the parentheses show the numbers of  $\alpha$  clusters. The characteristic features are the following: (1) There are stable energy pockets in all the cases, (2) the energy pocket is protected by the competition of the Coulomb repulsion and the Pauli principle, (3) the values of s.d. are almost the same for all the cases of energy pocket and barrier,

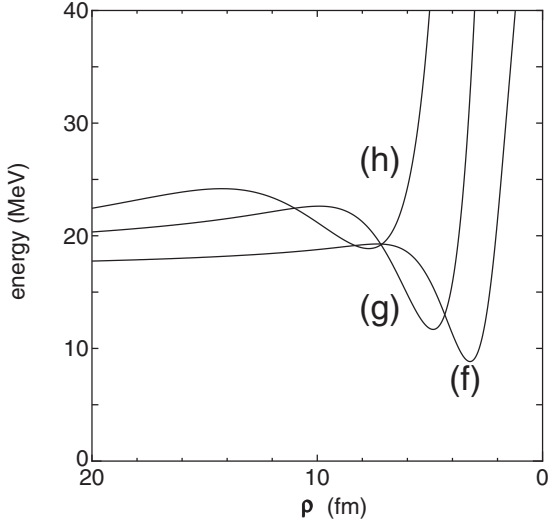


FIG. 3. Energy for one  $\alpha$  as a function of the radius ( $\rho$  in the text), (f) hexahedron-octahedron, (g) dodecahedron-icosahedron, and (h) fullerene.

but the rhombic triacontahedron and the fullerene shape have comparably large distance of two  $\alpha$  particles, (4) the Pauli index becomes almost 1 around the energy pocket, and the increase starts at the barrier position where the index is 0. We predict a void surrounded by  $\alpha$  particles, but we see that the gap of the

TABLE I. The physical quantities at the (A) barrier and (B) energy pocket positions calculated using F1 force. The radius ( $\rho$  in the text), depth of the energy pocket, and height of the barrier  $p_i(\rho)$  in Eq. (9) are listed. Here s.d. means the shortest distance of two  $\alpha$  clusters at the fixed radius of  $\rho$ . The values in parentheses show the energy after subtracting the center of mass kinetic energy for each  $\alpha$  cluster. Conf means configurations (a)–(h) in Fig. 1.

(A) Barrier	Conf	$\rho$ (fm)	s.d. (fm)	Height (MeV)	$p_i(\rho)$
P04(4)	(a)	4.5	7.35	8.845	0.000
P08(6)	(b)	5.2	7.35	12.071	0.000
P06(8)	(c)	6.0	6.93	13.814	0.000
P20(12)	(d)	6.7	7.05	16.180	0.000
P12(20)	(e)	9.0	6.42	18.367	0.004
P08-06(14)	(f)	7.3	6.71	19.271	0.001
P12-20(32)	(g)	9.9	6.41	22.626	0.011
Ful(60)	(h)	14.2	5.73	24.180	0.094
				(8.885)	
(B) Pocket	Conf	$\rho$ (fm)	s.d.(fm)	Depth (MeV)	$p_i(\rho)$
P04(4)	(a)	1.4	2.29	-3.039	0.994
P08(6)	(b)	2.1	2.97	-1.643	0.986
P06(8)	(c)	2.5	2.89	1.228	0.998
P20(12)	(d)	2.9	3.05	-0.367	1.000
P12(20)	(e)	3.9	2.78	6.700	1.000
P08-06(14)	(f)	3.2	2.94	8.838	1.000
P12-20(32)	(g)	4.9	3.14	11.694	1.000
Ful(60)	(h)	7.7	3.11	18.868	1.000
				(6.113)	

TABLE II. The physical quantities at the (A) barrier and (B) energy pocket positions calculated using Brink-Boeker force. The radius ( $\rho$  in the text), depth of the energy pocket, and height of the barrier  $p_i(\rho)$  in Eq. (9) are listed. Here s.d. means the shortest distance of two  $\alpha$  clusters at the fixed radius of  $\rho$ . The values in parentheses show the energy after subtracting the center of mass kinetic energy for each  $\alpha$  cluster. Conf means configurations (a)–(h) in Fig. 1.

(A) Barrier	Conf	$\rho$ (fm)	s.d. (fm)	Height (MeV)	$p_i(\rho)$
P04(4)	(a)	4.2	6.86	9.017	0.000
P08(6)	(b)	4.7	6.65	12.325	0.000
P06(8)	(c)	5.5	6.35	14.117	0.002
P20(12)	(d)	6.1	6.41	16.605	0.004
P12(20)	(e)	8.2	5.85	18.867	0.021
P08-06(14)	(f)	6.7	6.16	20.102	0.007
P12-20(32)	(g)	9.1	5.83	23.295	0.047
Ful(60)	(h)	12.7	5.13	25.189	0.384
				(10.379)	
(B) Pocket	Conf	$\rho$ (fm)	s.d. (fm)	Depth (MeV)	$p_i(\rho)$
P04(4)	(a)	2.0	3.27	3.200	0.732
P08(6)	(b)	2.3	3.25	4.732	0.936
P06(8)	(c)	2.8	3.23	8.458	0.972
P20(12)	(d)	3.1	3.26	7.841	0.999
P12(20)	(e)	4.9	3.50	15.803	0.997
P08-06(14)	(f)	3.6	3.31	16.079	0.998
P12-20(32)	(g)	5.3	3.40	18.540	1.000
Ful(60)	(h)	10.1	4.08	24.807	0.996
				(11.884)	

barrier height and the pocket decreases when the number of  $\alpha$  particles increases.

We show the same quantities as those in Table I for the case of BB force in Table II. The  $b$  parameter is taken to be 1.409 fm which gives the binding energy of 27.375 MeV for  $\alpha$  particle. Surprisingly enough, even fullerene-shaped  $\alpha$  clustering has an energy pocket; however, it is slightly shallower than the case of F1 force. On the other hand, the barrier position shifts inside. The general trends do not change so much compared with the case of F1 force, but physical quantities largely change. For instance, the tetrahedron shape correctly represents the ground state of  $^{16}\text{O}$ , which is well reproduced by the F1 force, but this configuration very much underbinds in the BB force case; the energy shows the value of unbound region.

All the quantities inevitably include the spurious c.m. energy of each  $\alpha$  particle to be removed due to the adiabatic treatment. The removal procedure is not so easy but possible. The values after subtracting center-of-mass motion of each  $\alpha$  cluster at energy barrier and pocket points are shown in the parentheses of Tables I and II. Since the vibration effect of each  $\alpha$  cluster is in three dimensions, the reduction of the kinetic energy is quite large (more than 10 MeV); however, the energy pocket does not disappear in F1 interaction case.

It is shown that  $\alpha$  clusters with geometric configurations have certain local energy pockets when they approach each other from large distances. These geometric configurations are favored when  $\alpha$  clusters form a nucleus; the Coulomb



TABLE III. Coulomb energy [Coul (MeV)] for one  $\alpha$  cluster at the energy pocket calculated using F1 force together with the radius parameter  $\rho$  (fm), which gives the energy pocket. Coul-WB is the Coulomb energy for four particles calculated using the Weizsäcker-Bethe mass formula. Conf means configurations (a)–(h) in Fig. 1.

	Conf	$\rho$ (fm)	Coul (MeV)	Coul-WB (MeV)
P04(4)	(a)	1.4	3.68	4.52
P08(6)	(b)	2.1	4.86	5.92
P06(8)	(c)	2.5	5.98	7.18
P20(12)	(d)	2.9	8.32	9.40
P12(20)	(e)	3.9	11.42	13.21
P08-06(14)	(f)	3.2	6.52	10.42
P12-20(32)	(g)	4.9	11.61	18.08
Ful(60)	(h)	7.7	19.90	27.50

repulsion, most important at large distances, is reduced by forming the hollow structures. This is shown by presenting the expectation values of the Coulomb interaction for all the geometric configurations at the energy pocket points. In Table III, the Coulomb energy [Coul (MeV)] for one  $\alpha$  cluster at the energy pocket calculated using F1 force are shown together with the radius parameter  $\rho$  (fm), which gives the energy pocket. These values are significantly smaller than Coul-WB, which is the Coulomb energy for four particles calculated using Weizsäcker-Bethe mass formula. Although the values of the optimal radius parameter  $\rho$  are not so large compared with the stand radius of nuclei with these mass numbers, the Coulomb energies are much smaller than the mass formula. Then the formation of geometric configuration and hollow structure is favored.

The nucleon number density of the fullerene configuration with  $\rho = 7.7$  fm is shown in Fig. 4 as a function of the radius. The integration over the radius is normalized to the number of nucleons, and we can clearly see the appearance of hollow structure.

In this Rapid Communication, full microscopic calculation (wave function is fully antisymmetrized and interaction is applied not between clusters but between nucleons) is carried out for the balloon-shaped  $\alpha$  clustering; typical eight examples, five platonic solids, two cases of dual polyhedra, and the fullerene shape are examined. It has been shown that  $\alpha$  clusters with these geometric configurations create certain local energy

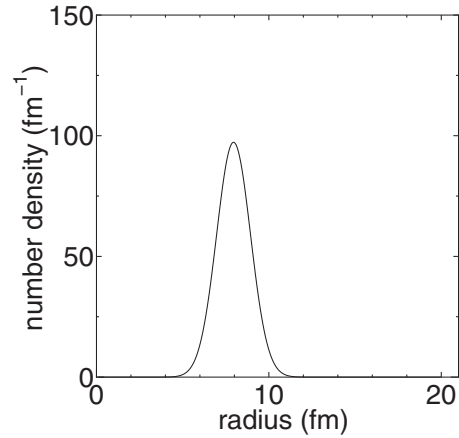


FIG. 4. Nucleon number density of the fullerene configuration with  $\rho = 7.7$  fm as a function of the radius. The integration over the radius is normalized to the number of nucleons.

pockets when they approach each other from large distances. These geometric configurations are favored when  $\alpha$  clusters form a nucleus; the Coulomb repulsion, most important at large distances, is reduced by forming the hollow structures. Here we avoid studying individual nuclei, because it is necessary to dynamically consider each nucleus, and this is another task. Namely, the next step of this investigation is to clarify the properties on individual nuclei. Is it crazy to imagine balloon nuclei which consist of  $\alpha$  clusters? Our answer is no. Reliable effective internucleon force and the complete consideration of the Pauli principle make it possible to give a correct answer. Surprisingly enough, the present report predicts that even ultra-super-heavy nuclei can exist with a void as local minimum configurations, when they gather from large distances.

One of the authors (A.T.) has discussed the fullerene-shaped  $\alpha$  clusters with the late W. Greiner, for whom the authors are now grateful. We also thank H. Horiuchi, Y. Funaki, P. Schuck, and G. Röpke for their fruitful discussions. Numerical calculation has been performed at Yukawa Institute for Theoretical Physics, Kyoto University. This work was supported by JSPS KAKENHI Grant No. 17K05440.

[1] R. Tamagaki, *Prog. Theor. Phys. Supplement* **E68**, 242 (1968).  
 [2] R. Tamagaki, *Prog. Theor. Phys.* **42**, 748 (1969).  
 [3] A. Tohsaki, H. Horiuchi, P. Schuck, and G. Röpke, *Phys. Rev. Lett.* **87**, 192501 (2001).  
 [4] Y. Funaki, H. Horiuchi, and A. Tohsaki, *Prog. Part. Nucl. Phys.* **82**, 78 (2015).  
 [5] Y. Fujiwara *et al.*, *Suppl. Prog. Theor. Phys.* **68**, 29 (1980).  
 [6] D. M. Brink, in *Proceedings of the International School of Physics “Enrico Fermi” Course XXXVI*, edited by C. Bloch (Academic Press, New York, 1966), p. 247.  
 [7] A. B. Volkov, *Nucl. Phys.* **74**, 33 (1965).  
 [8] A. Tohsaki, *Phys. Rev. C* **49**, 1814 (1994).  
 [9] N. Itagaki, *Phys. Rev. C* **94**, 064324 (2016).  
 [10] D. M. Brink and E. Boeker, *Nucl. Phys. A* **91**, 1 (1967).  
 [11] I. Tonzuka and A. Arima, *Nucl. Phys. A* **323**, 45 (1979).  
 [12] F. C. Chang, *Phys. Rev.* **155**, 1299 (1967).  
 [13] D. N. Poenaru and W. Greiner, in *Clusters in Nuclei I*, Lecture Notes in Physics Vol. 818, edited by C. Beck (Springer, Berlin, 2011), pp. 1–56.  
 [14] J. Zhang, W. D. M. Rae, and A. C. Merchant, *Nucl. Phys. A* **575**, 61 (1994).  
 [15] T. Neff and H. Feldmeier, *Nucl. Phys. A* **738**, 357 (2004).